

GCsT: Graph Convolutional Skeleton Transformer for Action Recognition

Ruwen Bai,^{1,2} Min Li,^{1,2} Bo Meng,³ Fengfa Li,^{1,2}
 Junxing Ren,^{1,2} Miao Jiang,^{1,2} Degang Sun^{1,2}

¹Institute of Information Engineering, Chinese Academy of Sciences, Beijing, China

²School of Cyber Security, University of Chinese Academy of Sciences, Beijing, China

³Beijing Institute of Technology, Beijing, China

bairuwen, limin@iie.ac.cn

Abstract

Graph convolutional networks (GCNs) achieve promising performance for skeleton-based action recognition. However, in most GCN-based methods, the spatial-temporal graph convolution lacks the flexibility of feature extraction caused by its neighborhood constraints of feature aggregations. In this paper, we present a novel architecture, named Graph Convolutional skeleton Transformer (GCsT), which can flexibly capture local-global contexts. In GCsT, Transformer and GCNs play complementary roles for feature representations. Hierarchical GCNs capture local topological information at varying levels. A spatial transformer attention module models the correlations between joint pairs in global topology, which relaxes the constraints of the graph convolution. A temporal transformer attention module is designed with long-short term attention, which learns all inter-frame dependencies effectively. GCsT has an effective combination of desirable properties, namely, dynamical attention and global context in Transformer, as well as hierarchy and local topology structure in GCNs. Furthermore, the proposed GCsT exhibits a stronger expressive capability by introducing additional information present in skeleton sequences. Incorporating Transformer allows that information to be naturally introduced into the model. As far as we know, this is the first work that a plug-and-play Transformer module is proposed to be integrated into GCNs for action recognition tasks. We validate the proposed GCsT by conducting extensive experiments, which achieves the state-of-the-art performance on NTU RGB+D, NTU RGB+D 120 and Northwestern-UCLA datasets.

Introduction

Human action recognition has been widely used in many applications such as intelligent video surveillance and smart retail. In the last few years, low-cost depth sensors like the Microsoft Kinect (Zhang 2012) and advanced estimation algorithms (Cao et al. 2019) have brought a considerable increase in available skeleton data, which enable great progress in skeleton-based action recognition. Among them, GCN-based methods have attracted a lot of attention due to their powerful capability to model the human topology graph. Yang et al. (Yan, Xiong, and Lin 2018) first built a spatial-temporal graph convolutional network (ST-GCN), in which each layer contains a graph convolutional block and a temporal convolutional block. ST-GCN has verified

the effectiveness of GCNs in modeling skeleton data but has several limitations. First, the graph topology based on the human body has strict neighborhood constraints on graph convolution operations at each layer in GCNs. Second, temporal convolutional operations can only process short-term skeleton sequences. Third, the model has the limited expressive power if only using joint position coordinates. In recent years, several GCN-based methods addressed these drawbacks from three aspects: (1) *Flexible graph construction* such as utilizing higher-order polynomial (Li et al. 2019b), adaptive (Shi et al. 2019) and multiscale (Liu et al. 2020) adjacency matrix; (2) *Long-term temporal dependencies modeling* such as applying multiscale temporal convolutional networks (MS-TCN), (Liu et al. 2020); (3) *Introducing additional information* such as bone (Shi et al. 2019) or motion information (Ye et al. 2020). Besides, some works (Li et al. 2019a) (Liu et al. 2020) considered the complex cross-spacetime joint connections but also brought an increase in the computational complexity and the number of model parameters. Instead of improving the expressiveness of exclusive GCNs, our work aims to employ Transformer to alleviate the above shortcomings in GCNs.

The main component in Transformer is self-attention, which computes the response at a position as a weighted sum of the features at all positions in the feature map. Unlike the self-attention operation, the spatial-temporal graph convolution operation used in GCNs is the weighted aggregation of node features in the local spatial-temporal neighborhood. The differences between the two operations give Transformer and GCN complementary expressive capabilities. The former captures long-range dependencies but does not inherently encode inductive biases to deal with structural data. The latter focuses on local spatial relationships and short-term temporal context while introducing topological priors into the network.

In this paper, we present a novel multi-stage hierarchy architecture called Graph Convolutional Skeleton Transformer (GCsT), as shown in Figure 1. The overall architecture is partitioned into three stages and each stage consists of two blocks. A spatial-temporal graph convolutional block (STGC) extracts the local-neighborhood relationships from the underlying graph topology, whereas a spatial-temporal Transformer block (STT) captures global space-time dependencies. Two blocks extract spatial-temporal features fol-

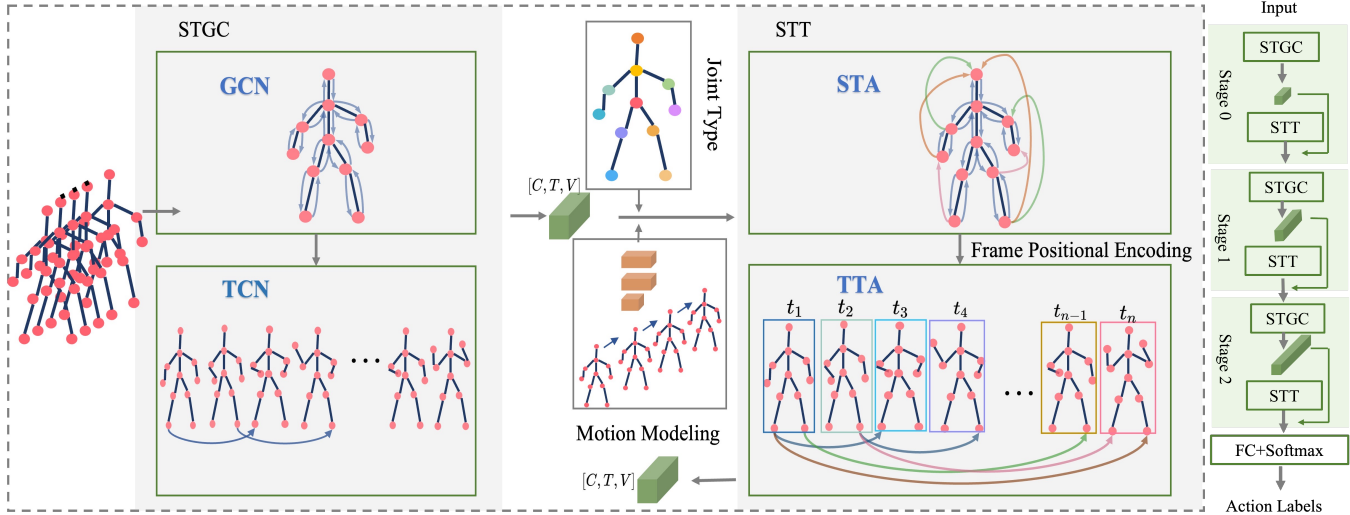


Figure 1: The overall architecture of the proposed Graph Convolutional Skeleton Transformer (GCsT). The three-stage architecture hierarchically extracts high-dimensional features from the input skeleton sequences. The residual connections ensure the transmission of local topological information. The details of the first stage are shown in the dashed box. In the first stage, we introduce three types of additional information to increase the richness of feature representation.

lowing the paradigm of stacking a spatial module (GCN or Spatial Transformer Attention (STA) module) and a temporal module (TCN or Temporal Transformer Attention (TTA) module). STA discovers the global correlations between bone-connected and actually unconnected joints, which relaxes the constraints of graph topology. TTA, a two-branch module, contains long-short term attention (LSTA). One branch specializes in the short-term temporal context modeling (by convolution) whereas another one specializes in the long-distance relationship modeling (by attention). Overall, GCsT can capture all dependencies in both local and global spatial-temporal contexts while paying dynamic attention to discriminative representations. Besides, hierarchical GCNs keep the local topological information at varying levels. Furthermore, a series of 2D or 3D coordinate positions only convey limited information. We believe that additional information in skeleton sequences always results in a more informative representation. In this work, we explicitly model the joint motion as well as embed high-level skeleton semantics (i.e. joint type and frame order) in the first stage of GCsT. The main contributions of our work are as follows:

- A novel architecture called GCsT is proposed, which employs all the benefits of Transformer (i.e. dynamical attention and global context) while keep the advantages of GCNs (i.e. hierarchy and local topology structure).
- A two-branch feature extractor, LSTA, is designed as the basic build block of our TTA, which captures all inter-frame dependencies effectively.
- Three kinds of information are introduced, namely, joint motion, joint type and frame order, which increase the richness of feature representation.
- Exhaustive ablation experiments are conducted to verify the effectiveness of our proposed GCsT, and results on

three datasets exceed the state-of-the-art methods.

Related Work

GCNs for skeleton-based action recognition. Recently GCNs have been widely adopted in skeleton-based action recognition due to its effective representation of the human body-based graph without losing topological information. In GCNs, graph topology determines whether correlation exists between joints. ST-GCN (Yan, Xiong, and Lin 2018) has drawn much attention to graph convolution, but in which graph topology is fixed and only models correlations between bone-connected joints. High-order adjacency matrix (Li et al. 2019b) and multiscale adjacency matrix (Liu et al. 2020) were introduced to aggregate joint features within a larger neighborhood. To model the hierarchical topology flexibly, an alternative approach is to adjust the topology graph dynamically during inference, such as using adaptive graph (Shi et al. 2019), A-links inference (Li et al. 2019b) and dynamic graph (Ye et al. 2020). Several studies (Li et al. 2019a; Liu et al. 2020) considered the information flow across space-time by the decomposed multiscale graph convolution and space-time graph convolution operators. These works tried to capture rich correlations between joints by learning the suitable graph topology. In our work, the graph topology is learned during training.

Transformer in Computer Vision. Recently, the breakthroughs from Transformer networks in natural language processing domain have sparked great interest in the computer vision community. The success of Transformers is attributed to global self-attention, which is the main component in Transformer. Self-attention operations have complementary advantages to convolutional operations, such as dynamic attention and global context fusion, while assum-

ing minimal inductive biases. The model CvT (Wu et al. 2021) combined convolutional neural network and Transformer in an efficient way, which model both local and global dependencies for image classification. Dynamical attention to global joints and frames from skeleton sequences allows the model to capture more informative correlations from given corresponding features. Inspired by this, incorporating Transformer in GCNs is considered in this work. A two-stream Transformer network for skeleton-based action recognition, ST-TR, was proposed(Plizzari, Cannici, and Matteucci 2021), which substitutes the regular graph convolutions on both space and time with the transformer self-attention operator. In contrast to ST-TR, we construct a multi-stage architecture in one stream. Each stage applies a plug-and-play spatial-temporal Transformer (STT) block with space-time mixing attention.

Method

In this section, basic graph convolution (Yan, Xiong, and Lin 2018) and standard Transformer (Vaswani et al. 2017) are first summarized. Then each component in our proposed model GCsT is introduced.

Preliminaries

GCN. The raw skeleton sequences are denoted as $X_{in} \in R^{C_{in} \times T \times N}$, where each vector $X_{in}^t = \{v_1^t, v_2^t, \dots, v_n^t\}$ represents the 2D or 3D coordinates of N human joints at a time stamp t . The basic spatial-temporal graph convolution operation at the l th layer is formulated as:

$$X^{l+1} = \sum_k^{K_v} W_k (X^l A_k) \quad (1)$$

With the partition strategy applied in ST-GCN, K_v is set to 3. W_k is a trainable weight matrix. Adjacency matrix $\bar{A}_k \in \{0, 1\}^{N \times N}$ represents the intrabody connections. $A_k = D_k^{-\frac{1}{2}} (\bar{A}_k + I) D_k^{-\frac{1}{2}}$ is the normalization of the adjacency matrix. Here, introducing the self-loop constant matrix I considers the influence of the node itself.

Transformer. The standard Transformer block is shown in Figure 2(a). Each block has two sublayers: a multihead self-attention layer (MHSA) and a fully connected feed-forward layer (FFN). The input sequences are first projected into three different matrices, queries $Q \in R^{N \times D_q}$, keys $K \in R^{N \times D_k}$, and values $V \in R^{N \times D_v}$, respectively. D_q , D_k , and D_v denote the dimensions of queries, keys and values. The scaled dot-product attention used by Transformer is computed as:

$$Attn = \text{softmax}\left(\frac{QK^T}{\sqrt{D_k}}\right)V \quad (2)$$

The MHSA mechanism project the D -dimensional representation into multiple subspaces with H different sets of learned projections. For each of the projected queries, keys and values, single attention head is computed according to Eq. 2. All attention heads are concatenated and projected back to D -dimensional representation, which can be formalized as:

$$MHSA(Q, K, V) = \text{Concat}(Attn_1, \dots, Attn_h)W^o \quad (3)$$

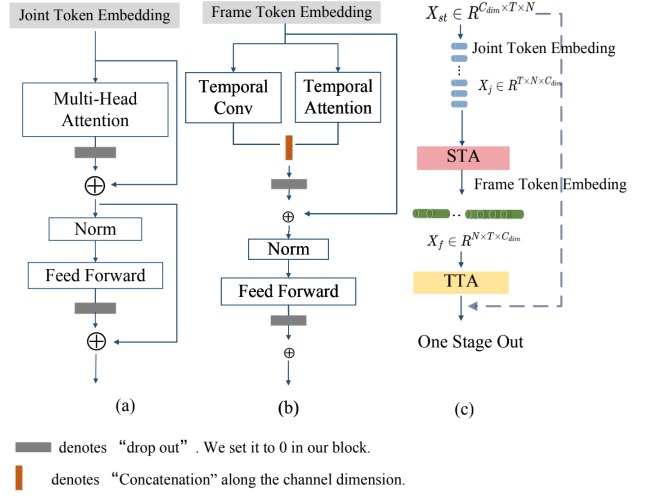


Figure 2: (a) Standard Transformer block and STA module used in this work; (b) TTA module; (c) Framework of STT block.

FFN consists of two-layer pointwise feedforward network. Transformer employs a residual connection around each module, followed by Layer Normalization. The entire process can be formulated as:

$$\begin{aligned} H' &= \text{LayerNorm}(MHSA(X) + X) \\ FFN(H') &= \sigma(H'W_1 + b_1)W_2 + b_2 \\ H &= \text{LayerNorm}(FFN(H') + H') \end{aligned} \quad (4)$$

where $X \in R^d$ is used as the input of self-attention layer, d_f is the dimensions of the transformation in FFN. $W_1 \in R^{d \times d_f}$ and $W_2 \in R^{d_f \times d}$ are the weight matrices, b_1 and b_2 are the bias vectors, and σ denotes the GELU activation function in our Transformer block. H denotes the final output of the standard Transformer block.

Spatial-Temporal GCN

Spatial-temporal graph convolution aims to extract spatial-temporal feature representations of joints at varying levels, from local spatial context to high-level action patterns. To model topology graph flexibility, adaptive graph convolution is adopted and formulated as:

$$X^{l+1} = \sum_k^{K_v} W_k^l X^l (\mathcal{M}_1 \mathcal{G}_k^a + \mathcal{M}_2 \mathcal{G}_k^s) \quad (5)$$

where, learnable weight W_k^l is unique for each layer. Adaptive graph topology contains two different types of topologies, namely, \mathcal{G}_k^a and \mathcal{G}_k^s .

Action-dependent Topology Learning. \mathcal{G}_k^a is parameterized and initialized to the adjacency matrix A_k , as introduced in Eq. 1. Therefore, the natural topology based on the human body dominates feature aggregation at the early stage of the training. When training stabilizes, \mathcal{G}_k^a dynamically infers the most suitable graph topology for all action categories according to the training data.

Sample-dependent Topology Learning. \mathcal{G}_k^s represents the sample-dependent topology, which models the correlations between the joints for each sample. Similar to recent works (Shi et al. 2019; Zhang et al. 2020), whether a connection exists between two joints (v_i, v_j) is determined here by computing the feature similarity of the joint pairs as:

$$S(v_i, v_j) = \theta(x_i)^T \phi(x_j), i, j \in 1, 2, \dots, N \quad (6)$$

where $x_i, x_j \in R^{C \times T \times N}$ are the corresponding features of joint pair (v_i, v_j) . Two linear transformations θ and ϕ embed joint features into low-dimensional embedding space $R^{C_d \times T \times N}$. Via modeling the correlations of all joint pairs for each sample, sample-dependent adjacency matrix \mathcal{G}_k^s are obtained by using *Tanh* activation function, θ .

Mask Refining Topology. A learnable mask \mathcal{M}_1 with an initialization value of 1 is added to change the importance of edges dynamically. Another learnable mask \mathcal{M}_2 is initialized to 0 so that the high-level feature representations of joints dominate the sample-dependent topology modeling. The intuition behind this is that higher-dimensional features represent more semantic information. \mathcal{M}_1 and \mathcal{M}_2 learn simultaneously and refine each other to relax the strict constraints of graph convolutions further. The learned topology enables dynamically modeling the correlations between any two bone connected or unconnected joints.

Spatial-Temporal Transformer Block

Spatial-temporal Token Embedding. The spatial-temporal features extracted by the STGC block will be first reshaped into joint tokens. Given that the output of the STGC block is $X_{st} \in R^{C_{dim} \times T \times V}$, it is reshaped into joint tokens, $X_j \in R^{T \times N \times C_{dim}}$, by moving the temporal dimension in the batch dimension, where C_{dim} , T , and V is the numbers of input feature channels, joints and frames respectively. Frame tokens $X_f \in R^{N \times T \times C_{dim}}$ are reshaped by the output from the previous STA block as shown in Figure 2(c). The token feature dimension and the numbers of frame tokens can be adjusted by varying the stride of the temporal convolution. The sequential setting is verified in experiments.

Spatial Transformer Attention Module The STA module is introduced to learn inter-joint dependencies dynamically. STA applies the standard Transformer block as shown in Figure 2(a). Spatial self-attention operates on joint tokens to consider all joints at the same timestamp, which is performed by MHSA. The *query* Q_j , *key* K_j , and *value* V_j representations are projected into different subspaces by applying multiple trainable transformations to joint tokens X_j . Each subspace has the same embedding dimensions. The computation of STA is the same as that of the standard Transformer block. The self-attention computation in STA captures how much attention one joint pays to any other joint, breaking the neighborhood restriction in the graph convolution.

Temporal Transformer Attention Moudle Self-attention computes the pairwise dot-product between all the input elements to model global context relationships. Despite its

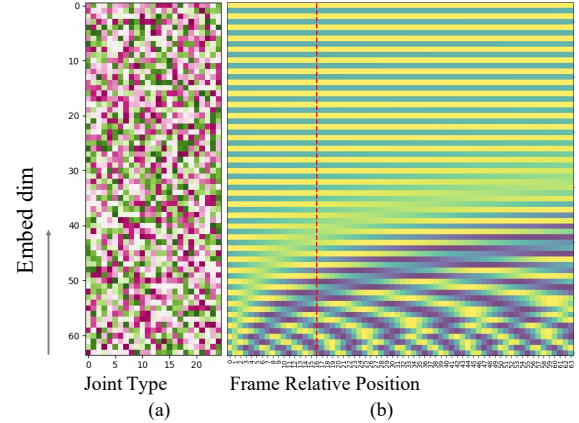


Figure 3: Visualization of the embedding feature maps of the joint type (a); and the frame order(b). The red line indicates the order of the 16th frame.

effectiveness, self-attention in Transformer causes the deficiency of local context (Fan et al. 2021). For the TTA module, a new design is presented to strengthen Transformer in localness modeling while keeping global context relationships.

Instead of the standard self-attention mechanism, TTA follows a two-branch design, as shown in Figure 2(b). One branch captures the short-term inter-frame context by using the temporal convolution layer and another branch models the long-term temporal dependencies. Specially, the input channels are split into two parts. The output feature maps from the two branches are concatenated and fed into the FFN layers. The temporal convolution enables the capture of local temporal context. Another branch applies a standard MHSA to learn temporal dependencies globally. The concatenated feature maps represent long-short term relations with 2 times reduced computations. Moreover, a temporal convolution with stride 2 in the STGC block is used in the last two stages. The computational efficiency of TTA with a reduced number of frame tokens also benefits from such multi-stage hierarchical structure.

Introducing Additional Information

The Positional Encoding of Transformer allows introducing some sense of joint type and frame order without any efforts. In this work, we introduce additional information, namely, joint type, joint motion and frame order, to enlarge the model’s expressive power. The information only needs to be introduced in the first stage, which is reasonable because the hierarchical architecture and residual connections are sufficient to keep the information flow.

Joint Type Embedding. Different joint types represent the semantics of various body parts. Taking 25 joints in NTU RGB+D (Shahroudy et al. 2016) as an example, the 3rd joint indicates the “neck”. We embed C_e dimensions of feature representations for each joint type, thus $J_{embed} \in R^{N \times C_e}$. The visualization of J_{embed} is shown in Figure 3(a), which is distinct for each joint type.

Joint Motion Modeling. Given the feature representation $X \in R^{C_m \times T \times N}$, a linear transformation with reduction rate r is utilized to reduce computation cost before computing the motion feature: $X^r = WX, X^r \in R^{C_m/r \times T \times N}$. The joint motion representations at time step t are approximately considered the difference between the two adjacent frames, $X_t^r, X_{t-1}^r \in R^{C_m/r \times (T-1) \times N}$. The motion is encoded using two 1×1 2D convolution layers, which expands the dimensions of feature channels to the original channel dimension C_m , which can be written as:

$$J_m = \sigma(W_{m2}\sigma(W_{m1}((X_t^r - X_{t-1}^r) + b_{m1}) + b_{m2}) \quad (7)$$

where $W_{m1} \in R^{C_m \times (C_m/r)}$, $W_{m2} \in R^{C_m \times C_m}$ and σ is the *ReLU* activation function.

Frame Order Embedding. The frame position in skeleton sequences represents the frame order in time, which contains high-level semantics related to actions. We utilize sinusoidal positional encoding introduced by (Vaswani et al. 2017), which gives the order context of frames effortlessly. The visualization of \vec{p}_t is shown in Figure 3(b).

Experiments

We evaluate the proposed GCsT on NTU RGB+D (Shahroudy et al. 2016), NTU RGB+D 120 (Liu et al. 2019), and Northwestern-UCLA datasets (Wang et al. 2014).

Datasets

NTU RGB+D (NTU 60). NTU RGB+D is a human action dataset with 60 categories collected by Microsoft Kinect V2, which contains 3D joint coordinates of 25 body joints. The dataset collects 56,880 video samples in total from 40 subjects. Two benchmarks are recommended for evaluation: (1) Cross-subject (X-Sub): training data comes from 20 subjects, and testing data comes from the other 20 subjects. (2) Cross-view (X-View): training data comes from camera views 2 and 3, and testing data comes from camera view 1.

NTU RGB+D 120 (NTU 120). This dataset extends NTU 60 with an additional 57,367 skeleton sequences over 60 extra action classes, totalling 113,945 samples over 120 classes captured from 32 different camera setup and 106 volunteers. It is currently the largest skeleton dataset with 3D joints annotations. Two benchmarks are recommended for evaluation: (1) cross-subject (X-Sub): 63,026 samples from a selected group of 53 subjects are used for training, and the rest 50,919 samples for testing. (2) cross-setup (X-Setup): 54,468 samples collected from half of the camera setups are used for training and the rest 59,477 samples for testing.

Northwestern-UCLA (NW-UCLA). Northwestern-UCLA dataset is captured by three Kinect cameras. This dataset collects 1494 video clips covering 10 action categories, which are performed by 10 actors. The same evaluation protocol in (Wang et al. 2014) is adopted here: training data from the first two cameras, and testing data from the other camera.

Implementation Details

All experiments are conducted on two RTX TITAN GPUs with the PyTorch framework. We use SGD with momentum (0.9) to train the model for 60 epochs. Cross entropy loss is utilized with 0.1 label smoothing rate. The initial learning rate is 0.05 and reduced by 10 at the 40th and 50th epochs. The weight decay is set to 0.0001. For NTU 60/120, the batch size is 64. The raw skeleton sequences are downsampled to a fixed size of 64 frames. Data preprocessing is conducted with the same strategy as introduced in (Li et al. 2019a). For NW-UCLA, the batch size is 16, we adopt the data pre-processing in (Cheng et al. 2020b).

Ablation Study

We design elaborate ablation experiments to investigate the effectiveness of GCsT. Unless stated, performance is reported as classification accuracy on X-View benchmark of NTU60 using only the joint data. ST-GCN is employed as the baseline.

Topology Learning in STGC We first validate the effects of action-dependent topology learning (\mathcal{G}_k^a) and sample-dependent topology learning (\mathcal{G}_k^s) respectively. Then we test the performance of learning two types of topologies together as well as adding each of two masks, \mathcal{M}_1 and \mathcal{M}_2 . The results are shown in Table 1. *w* denotes “with”. It suggest that the human body structure always benefits topology learning. When topology is learned without any restriction of the human body structure, the performance of GCsT drops by 0.6% both with joints only and with joints and bones (Table 1b v.s. Table 1f). If mask \mathcal{M}_2 is added to refine the sample-dependent topology learning according to the high-dimensional feature maps, the performance is slightly better (+ 0.2% (Joint), 0.3% (w Bone)) (Table 1d v.s. Table 1e). Mask \mathcal{M}_1 relaxes the constraints of the underlying structure and our GCsT obtains the best performance (Table 1f).

Method	Topology Learning				Acc(%) (Joint)	Acc(%) (w Bone)
	\mathcal{G}_k^a	\mathcal{G}_k^s	\mathcal{M}_1	\mathcal{M}_2		
a	✓				94.8	95.9
b		✓			94.7	95.6
c	✓		✓		95.2	95.9
d	✓	✓			94.9	95.7
e	✓	✓		✓	95.1	96.0
f	✓	✓	✓	✓	95.3	96.2

Table 1: Comparisons of the validation accuracy(%) of GCsT with different topology learning on NTU 60 (X-View).

Figure 4 illustrates three learned topologies at the first and last stage. Three topology learning methods “a, d, and f” correspond to “a,d, and f” in Table 1. The darkness of the color indicates the strength of the connection. The 2nd row shows that the correlations between low-level joint features gradually conceal the information of the topology structure from the first stage. The final learned topology balances the global joint associations with the local information in the topological structure. It suggests that Transformer relaxes the strict

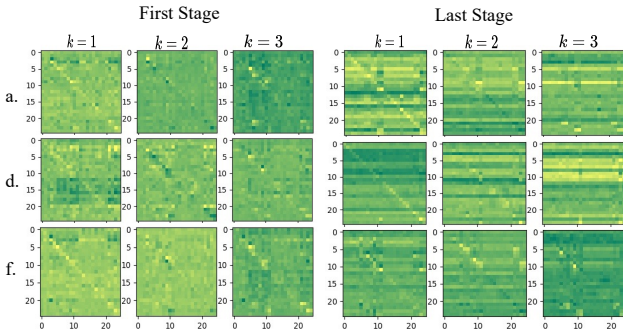


Figure 4: Visualization of three kinds of learned topologies in two stages of our model. “a, d, and f” correspond to the topology learning method in the Table 1, “a, d, and f”. k denotes the different subsets of the learned topology.

constraints on the neighborhood caused by graph convolution effectively, as well as highlights the discriminative information.

Spatial-temporal Attention in STT In this part, we conduct experiments on several variants of GCsT to validate the effectiveness of each module in the STT block. The results are shown in Table 2. We first test the contributions of two modules, STA and TTA, shown as *A. GCsT w STA* and *B. GCsT w TTA*, respectively. Our proposed method substantially improves the action recognition task by only using STA or TTA. It suggests that attention to all joints and sequential frames consistently contributes greatly to action recognition. To validate the capability of our proposed TTA, two variants are examined: *C. GCsT w TTA-L*: The long-short term TTA module is replaced with a standard long-term temporal Transformer. *D. GCsT w MS-TCN*: The TCN module in STGC is replaced with MS-TCN (introduced in (Liu et al. 2020)). The performance drops by 0.7% and 0.6%, respectively, showing that TTA with long-short term attention captures all inter-frame dependencies effectively. Furthermore, we test two different loading modes of STA and TTA in STT, namely, sequentially or in parallel, shown as *E. GCsT w STT-S* and *F. GCsT w STT-P*, respectively. Sequential loading achieves a slightly better performance. Finally, we combine STT with the basic GCN in ST-GCN (shown in Table 3), which also brings encouraging improvements of 4.7% and 2.1% on X-Sub and X-View benchmarks, respectively. It suggests that STT is plug-and-play and can be flexibly combined with any GCN, which further confirms our motivation.

Effect of Additional Information The effectiveness of each information introduced in our model is validated by removing one alone and the results are shown in Table 4. The absence of any kind of information would lead to a drop in accuracy. We observe that the joint type is as important a part of our model as the frame order. Performance drops by 1.1% when we remove the joint motion modeling, which indicates the importance of modeling the short-term joint motion. We believe that the joint motion modeling prompts TTA to re-

Methods	Params($\times 10^5$)	Acc(%)
Baseline	31.0	92.7
<i>A. GCsT w STA</i>	15.8	95.0
<i>B. GCsT w TTA</i>	14.1	94.9
<i>C. GCsT w TTA-L</i>	21.2	94.6
<i>D. GCsT w MS-TCN</i>	12.8	94.7
<i>E. GCsT w STT-S</i>	19.4	95.3
<i>F. GCsT w STT-P</i>	19.4	95.1

Table 2: Comparison of the validation accuracy for several variants of GCsT on NTU 60 (X-View).

Methods	Params	X-Sub(%)	X-View(%)
Baseline	31.0	84.3	92.7
Basic GCN+STT	18.4	89.0	94.8
GCsT	19.4	89.7	95.3

Table 3: Comparison between the combination of the basic GCN with STT and GCsT on NTU 60.

Method	Joint Type	Joint Motion	Frame Relative Position	Param ($\times 10^5$)	Acc(%)
a		✓	✓	19.4	95.0
b	✓		✓	19.3	94.2
c	✓	✓		19.4	94.9
f	✓	✓	✓	19.4	95.3

Table 4: Comparison of the validation accuracy on NTU 60 (X-View) when removing one from the added information.

tain more dynamics between neighboring frames. The model parameters increase very slightly after introducing information.

Vsualization of GCsT

In Figure 5(a), the relationships between all joint pairs in space and all frames in time are considered by the self-attention computation in Transformer. Figure 5 shows the learned feature maps of five action samples. The size of the pink circle represents the intensity of feature responses. The large pink circle indicates the informative joints. The orange circle highlights the strong connected joint pairs. The lines other than bones represent the attention connections, and the 10 largest scores are taken for visualization. The thickness of the lines represents the level of attention score. The selected joints by our GCsT for five actions are consistent with human intuition. For example, strong connections exist between the head and the foot. “Kicking” needs the coordination of the left foot with other body parts.

Comparison with the State-of-the-arts

The proposed GCsT is compared with other models when using two different data modalities on NTU 60, NTU 120, and NW-UCLA. On NTU 60 (Table 5), both with joint only and with combined joint and bone information, our GCsT achieves state-of-the-art performance on X-Sub and X-View benchmarks. HCN (Li et al. 2018) and ST-GCN are two rep-

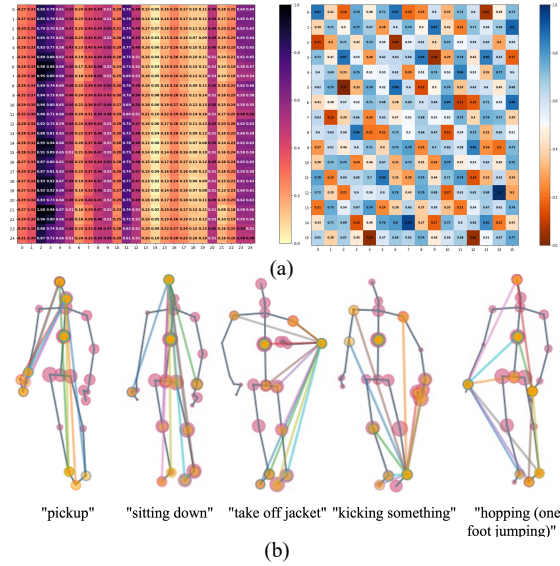


Figure 5: (a) Example of attention scores of an action sample “pick up:” the upper left is spatial attention scores between all joint pairs, and the upper right is temporal attention scores between frames; (b) Examples of feature response maps and learned spatial attention connections.

NTU RGB+D 60		
Methods	X-Sub	X-View
HCN (Li et al. 2018)	86.5	91.1
ST-GCN (Yan, Xiong, and Lin 2018)	81.5	88.3
AS-GCN (Li et al. 2019b)	86.8	94.2
STGR-GCN (Li et al. 2019a)	86.9	92.3
SGN (Zhang et al. 2020)	89.0	94.5
2s-AGCN (Shi et al. 2019)	88.5	95.1
4s-Shift GCN (Cheng et al. 2020b)	90.7	96.5
MS-G3D (Liu et al. 2020)	91.5	96.2
Dynamic GCN (Ye et al. 2020)	91.5	96.0
ST-TR(Joint)	88.7	95.6
ST-TR(Joint+Bone)	89.9	96.1
ST-TR-agcn(Joint)	89.2	95.8
ST-TR-agcn(Joint+Bone) (Plizzari, Cannici, and Matteucci 2021)	90.3	96.3
GCsT (Joint)	89.7	95.3
GCsT (Joint+Bone)	91.6	96.2

Table 5: Comparison with the state-of-the-art accuracy (%) on NTU 60.

representative methods for CNN-based and GCN-based methods, and GCsT outperforms them by 5.1% and 10.1% respectively. On X-Sub benchmark, when using bone information, our model shows superior performance with improvements of 1.7% and 1.3% compared with ST-TR and ST-TR-agcn, respectively. To the best of our knowledge, ST-TR and ST-TR-agcn are the only existing models that employ Transformer in skeleton action recognition. On X-View benchmark, the performance of GCsT is on-par with the current state-of-the-art methods MS-G3D (Liu et al. 2020) and Dy-

NTU RGB+D 120		
Methods	X-Sub	X-Set
SGN (Zhang et al. 2020)	79.2	81.5
2s-AGCN (Shi et al. 2019)	82.9	84.9
4s-shift GCN (Cheng et al. 2020b)	85.9	87.6
MS-G3D (Liu et al. 2020)	86.9	88.4
Dynamic GCN (Ye et al. 2020)	87.3	88.6
ST-TR	84.3	86.7
ST-TR-agcn (Plizzari, Cannici, and Matteucci 2021)	85.1	87.1
GCsT(Ours)	87.7	89.3

Table 6: Comparison with state-of-the-art accuracy (%) on NTU 120.

Northwern-UCLA	
Methods	Top-1
Lie Group (Veeriah, Zhuang, and Qi 2015)	74.2
Actionlet ensemble (Wang et al. 2013)	76.0
HBRNN-L (Du, Wang, and Wang 2015)	78.5
Ensemble TS-LSTM (Lee et al. 2017)	89.2
AGC-LSTM (Si et al. 2019)	93.3
4s-shift GCN (Cheng et al. 2020b)	94.6
DC-GCN+ADG (Cheng et al. 2020a)	95.3
GCsT(Ours)	96.1

Table 7: Comparison with state-of-the-art accuracy (%) on NW-UCLA.

namic GCN (Ye et al. 2020). The slightly lower accuracy than 4s-Shift GCN (Cheng et al. 2020b) is attributed to two additional streams in 4s-Shift GCN dedicated to modeling joint motion and bone motion information. On NTU 120 and NW-UCLA (Table 6, 7), our model achieves the best accuracy, exceeding all previously reported performance.

Conclusion

In this paper, we propose a novel architecture GCsT for skeleton-based action recognition, which makes full use of the complementary properties in Transformer and hierarchical GCNs. Extensive experiments are conducted to verify the effectiveness of the design of GCsT. Our GCsT capture all discriminative information in space and time from local neighborhood and global context. Incorporating Transformer gives us the ability to introduce additional information present in skeleton sequences without placing extra burdens on the model. A comprehensive discussion and visualization demonstrate that our GCsT allows for more flexibility, richness and discrimination in feature representations. On three datasets, GCsT achieves the state-of-the-art performance.

References

Cao, Z.; Hidalgo, G.; Simon, T.; Wei, S.-E.; and Sheikh, Y. 2019. OpenPose: realtime multi-person 2D pose estimation using Part Affinity Fields. *IEEE transactions on pattern analysis and machine intelligence*, 43(1): 172–186.

Cheng, K.; Zhang, Y.; Cao, C.; Shi, L.; Cheng, J.; and Lu, H. 2020a. Decoupling gcn with dropgraph module for skeleton-

based action recognition. In *Computer Vision–ECCV 2020: 16th European Conference, Glasgow, UK, August 23–28, 2020, Proceedings, Part XXIV 16*, 536–553. Springer.

Cheng, K.; Zhang, Y.; He, X.; Chen, W.; Cheng, J.; and Lu, H. 2020b. Skeleton-based action recognition with shift graph convolutional network. In *Proceedings of the IEEE/CVF Conference on Computer Vision and Pattern Recognition*, 183–192.

Du, Y.; Wang, W.; and Wang, L. 2015. Hierarchical recurrent neural network for skeleton based action recognition. In *Proceedings of the IEEE conference on computer vision and pattern recognition*, 1110–1118.

Fan, Z.; Gong, Y.; Liu, D.; Wei, Z.; Wang, S.; Jiao, J.; Duan, N.; Zhang, R.; and Huang, X. 2021. Mask Attention Networks: Rethinking and Strengthen Transformer. *arXiv preprint arXiv:2103.13597*.

Lee, I.; Kim, D.; Kang, S.; and Lee, S. 2017. Ensemble deep learning for skeleton-based action recognition using temporal sliding lstm networks. In *Proceedings of the IEEE international conference on computer vision*, 1012–1020.

Li, B.; Li, X.; Zhang, Z.; and Wu, F. 2019a. Spatio-temporal graph routing for skeleton-based action recognition. In *Proceedings of the AAAI Conference on Artificial Intelligence*, volume 33, 8561–8568.

Li, C.; Zhong, Q.; Xie, D.; and Pu, S. 2018. Co-occurrence feature learning from skeleton data for action recognition and detection with hierarchical aggregation. *arXiv preprint arXiv:1804.06055*.

Li, M.; Chen, S.; Chen, X.; Zhang, Y.; Wang, Y.; and Tian, Q. 2019b. Actional-structural graph convolutional networks for skeleton-based action recognition. In *Proceedings of the IEEE/CVF Conference on Computer Vision and Pattern Recognition*, 3595–3603.

Liu, J.; Shahroudy, A.; Perez, M.; Wang, G.; Duan, L.-Y.; and Kot, A. C. 2019. Ntu rgb+ d 120: A large-scale benchmark for 3d human activity understanding. *IEEE transactions on pattern analysis and machine intelligence*, 42(10): 2684–2701.

Liu, Z.; Zhang, H.; Chen, Z.; Wang, Z.; and Ouyang, W. 2020. Disentangling and unifying graph convolutions for skeleton-based action recognition. In *Proceedings of the IEEE/CVF Conference on Computer Vision and Pattern Recognition*, 143–152.

Plizzari, C.; Cannici, M.; and Matteucci, M. 2021. Spatial temporal transformer network for skeleton-based action recognition. In *International Conference on Pattern Recognition*, 694–701. Springer.

Shahroudy, A.; Liu, J.; Ng, T.-T.; and Wang, G. 2016. Ntu rgb+ d: A large scale dataset for 3d human activity analysis. In *Proceedings of the IEEE conference on computer vision and pattern recognition*, 1010–1019.

Shi, L.; Zhang, Y.; Cheng, J.; and Lu, H. 2019. Two-stream adaptive graph convolutional networks for skeleton-based action recognition. In *Proceedings of the IEEE/CVF Conference on Computer Vision and Pattern Recognition*, 12026–12035.

Si, C.; Chen, W.; Wang, W.; Wang, L.; and Tan, T. 2019. An attention enhanced graph convolutional lstm network for skeleton-based action recognition. In *Proceedings of the IEEE/CVF Conference on Computer Vision and Pattern Recognition*, 1227–1236.

Vaswani, A.; Shazeer, N.; Parmar, N.; Uszkoreit, J.; Jones, L.; Gomez, A. N.; Kaiser, Ł.; and Polosukhin, I. 2017. Attention is all you need. In *Advances in neural information processing systems*, 5998–6008.

Veeriah, V.; Zhuang, N.; and Qi, G.-J. 2015. Differential recurrent neural networks for action recognition. In *Proceedings of the IEEE international conference on computer vision*, 4041–4049.

Wang, J.; Liu, Z.; Wu, Y.; and Yuan, J. 2013. Learning actionlet ensemble for 3D human action recognition. *IEEE transactions on pattern analysis and machine intelligence*, 36(5): 914–927.

Wang, J.; Nie, X.; Xia, Y.; Wu, Y.; and Zhu, S.-C. 2014. Cross-view action modeling, learning and recognition. In *Proceedings of the IEEE conference on computer vision and pattern recognition*, 2649–2656.

Wu, H.; Xiao, B.; Codella, N.; Liu, M.; Dai, X.; Yuan, L.; and Zhang, L. 2021. Cvt: Introducing convolutions to vision transformers.

Yan, S.; Xiong, Y.; and Lin, D. 2018. Spatial temporal graph convolutional networks for skeleton-based action recognition. In *Proceedings of the AAAI conference on artificial intelligence*.

Ye, F.; Pu, S.; Zhong, Q.; Li, C.; Xie, D.; and Tang, H. 2020. Dynamic GCN: Context-enriched topology learning for skeleton-based action recognition. In *Proceedings of the 28th ACM International Conference on Multimedia*, 55–63.

Zhang, P.; Lan, C.; Zeng, W.; Xing, J.; Xue, J.; and Zheng, N. 2020. Semantics-guided neural networks for efficient skeleton-based human action recognition. In *Proceedings of the IEEE/CVF Conference on Computer Vision and Pattern Recognition*, 1112–1121.

Zhang, Z. 2012. Microsoft kinect sensor and its effect. *IEEE multimedia*, (2): 4–10.